Pré-filtrage en champ lointain pour l'analyse du bruit de jet

Maxime Koenig, André Cavalieri, Peter Jordan, Joël Delville, Yves Gervais, Mo Samimy, Sanjive Lele

10ème **C**ongrès **F**rançais d'**A**coustique

Lyon, 12-16 Avril 2010

Pré-filtrage en champ lointain pour l'analyse du bruit de jet

Maxime Koenig[1,2], André V. G. Cavalieri[1,3], Peter Jordan[1],
Joël Delville[1], Yves Gervais[1], Mo Samimy[4] et Sanjive Lele[5]

[1] Institut PPRIME, CNRS - Université de Poitiers - ENSMA, UPR 3346, Département Fluides, Thermique, Combustion, CEAT - 43 rue de l'aérodrome, F-86036 Poitiers Cedex France, maxime.koenig@lea.univ-poitiers.fr

[2] SNECMA, Acoustics Department, 77550 Moissy-Cramayel, France

[3] Instituto Tecnológico de Aeronáutica, São José dos Campos, Brazil

[4] The Ohio State University, Columbus, OH, USA

[5] Stanford University, Stanford, CA, USA

We present an analysis of the sound field radiated by a high Mach number subsonic jet. The spatial and temporal structures of the sound field are filtered and studied, respectively, by means of Proper Orthogonal Decomposition (POD) and wavelet transforms. The first POD mode is shown to give a near-perfect representation of the fluctuation energy radiation at low angles (in the range $30^\circ \leq \theta \leq 50^\circ$), larger numbers of modes being necessary to completely reproduce the radiation characteristics at higher angles. The wavelet analysis shows, in agreement with previous studies, that the temporal structure of the sound field is characterised by localised high-amplitude events. We implement two threshold intermittency metrics which we use to filter the pressure signals based on the scalogram topology. By varying these metrics we endeavour to characterise the intermittency of the pressure signals as a function of emission angle. We again find that the sound field can be divided into two families : the fluctuations radiated at low angles ($30^\circ \leq \theta \leq 50^\circ$) are characterised by higher levels of global intermittency (an intermittency metric defined with respect to the overall fluctuation energy) than the fluctuations radiated in the angular range $\theta > 50°$. However, when Farge's Local Intermittency Measure (defined with respect to the local fluctuation energy at each scale) is used to analyse the data, the fluctuations at all angles show identical behaviour.

1 Introduction

A striking characteristic of the sound field radiated by a jet is the angular dependence of the power spectrum, and this has led to the idea that there may be two different 'source' mechanisms at work in the production of sound by high-speed subsonic flows (see Tam [1]). However, as argued in the review paper of Jordan and Gervais [2], while Tam's similarity spectra clearly hint at an intriguing peculiarity regarding the behaviour of a jet flow in the production of sound, the precise details of what this peculiar behaviour entails remain unclear. The recent paper by Tam et al. [1] argues for the existence of two distinctly different, statistically independent, kinds of 'source' activity, while other recent work by Leib & Goldstein [3] demonstrates that the farfield structure may also be explained by appealing to a difference in the way a single 'source' structure 'couples' with the farfield.

As early as 1972 (Crow [4], Michalke [5]) the idea that coherent structures in jets may radiate in a manner similar to that of a convected wave-packet has been considered. Since that time, a considerable number of studies have pursued this line of thought. Tam et al. use this analogy to explain the downstream radiation pattern of a jet, arguing that the sideline radiation is a result of statistically independent 'fine-scale' turbulence. It is interesting to ask two questions with regard to such descriptions of sound-sources in jets. Firstly, does farfield data support the idea of two statistically independent source mechanisms ? And, secondly, what are the salient features of such sources, if they exist ? For example, in the case of the wave-packet source, the answer to the second question which is most often provided appeals to the effect of spatial amplitude modulation, which, on account of the antenna-effect leads to constructive interference, resulting in a 'beaming' of sound energy in the downstream direction ; in the spectral domain this amounts to the appearance of fluctuation energy with sonic phase velocity in the radiation direction(s).

A further interesting characteristic of sound production by subsonic round jets, which has been recognised for some time (Juvé et al. [6], Guj et al. [7], Hileman et al. [8]), and which is now receiving closer attention, in terms of both analysis (Cavalieri et al. [9]) and modelling (Sandham et al. [10], Cavalieri et al. [11]), is its temporal intermittency : the most energetic sound producing events occur in temporally localised bursts. This means that Fourier frequency analysis is poorly adapted for an optimal description of both 'source' and sound : the projection of the space-time structure of either onto infinitely extended Fourier modes will tend to 'smear' the local details of the sound-production events across a large band of frequencies ; the most salient local de-

tails may thus be hidden. Furthermore, this observation raises the question : is jet-noise really as broadband as the Fourier spectrum suggests - the spatiotemporal jittering of a small number of spatiotemporally localised, coherent events can produce a deceptively broad spectrum.

In this paper we address the above questions by effecting decompositions of the farfield radiated by subsonic jets. We endeavour to do so in as objective and unbiased a manner as possible. We choose Proper Orthogonal Decomposition to assess the spatial structure of the farfield, and wavelet transforms to assess the temporal structure. Each tool is used to ask a specific question. In the case of POD our reasoning is as follows : if statistically independent source mechanisms are simultaneously operative within a jet, it should be possible to discern this purely by statistical analysis of simultaneous multi-microphone data. The simplest and arguably least biased approach is to look at the POD modes (or principal components) of the data. How effective are the POD modes in compressing, i.e. explaining or fitting, the instantaneous pressure data ? In the case of the wavelet decomposition, we seek to quantify the temporal intermittency of the farfield as a function of polar angle.

By means of these analysis procedures it is possible to decompose the farfield into different components : the POD analysis allows a decomposition into a component associated with the first principal component of the farfield (the 1st POD mode) and a residuum (all of the other modes) ; the wavelet analysis allows the farfield to be decomposed into components associated with the high-energy bursts and a residuum. By performing these filtering operations we show that the POD filtering allows us to split the farfield into two families : the first POD mode captures nearly all of the fluctuation energy radiated in the angular sector $30^\circ \leq \theta \leq 50^\circ$, fluctuations at higher angles being shared among a larger number of modes. The wavelet filtering shows that when an intermittency metric is defined with respect to the total fluctuation energy we again observe a division of the data into the same pair of angular sectors.

2 Experiment

The experiments reported here were performed at the MARTEL facility of CEAT (Centre d'Etudes Aérodynamiques et Thermiques), Poitiers, France on a 0.05 m diameter cold jet at Mach 0.9 and high Reynolds number (10^6). The acoustic field was sampled using an arc of 12 microphones at a distance of 30 diameters from and centred on the jet exit. The angular position of the microphones varies from 30° to 140° with respect to the downstream jet axis. The acoustic setup is shown in figure 1. For further details see Jordan et al [12].

The Power spectra for the 12 microphones is shown in figure 2. The characteristic LSS (Large-Scale Spectrum) and FSS (Fine-Scale Spectrum) shapes are observed, respectively, at low and high emission angles (see Tam [1] for more details).

FIG. 1: Experiment in the MARTEL facility.

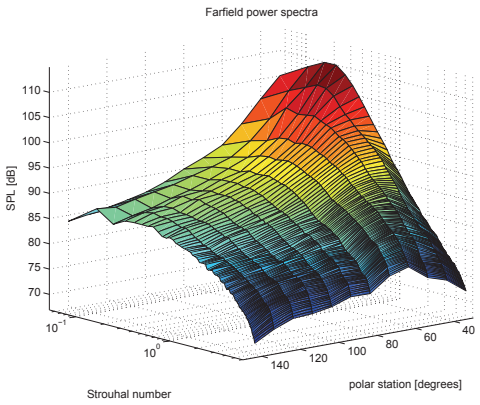

(a)

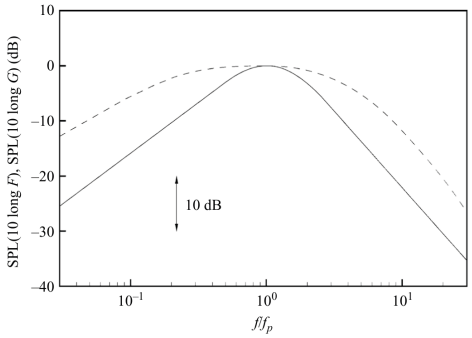

(b)

FIG. 2: (a) Power spectra of the Mach 0.9 jet ; (b) Tam's [1] similarity spectra.——, LSS spectra ;— – —, FSS spectra.

3 Analysis methodology

As outlined in the introduction, we aim to study and subsequently decompose the farfield of the jet by appealing to both its spatial (polar) and temporal structures. POD and wavelet transforms are used to achieve this.

3.1 POD analysis

In the case of farfield jet noise, temporal POD (whose Kernel is a spatial correlation at zero time-delay $p(\theta_i, \tau_i = 0)p(\theta_j, \tau_j = 0)$) is of limited use, because the microphone signals are more or less de-correlated at zero time delay. The cross-correlation matrix is therefore diagonal, the corresponding eigenfunctions resemble Dirac functions (each with a peak at a given microphone location), and the spectra of the expansion coefficients correspond, approximately, to the microphone spectra.

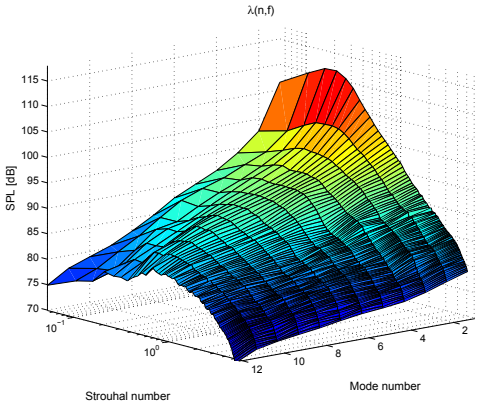

(a)

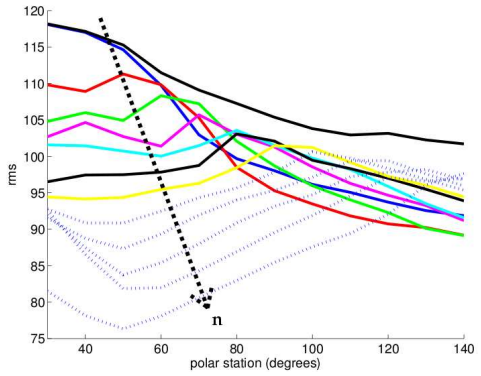

(b)

FIG. 3: (a) Eigenspectra, $\lambda_i(f)$; (b) rms (total and per n) ; black line = sum of POD modes ; colored lines = contribution of each POD mode ; Blue : n=1 ; Red : n=2, ...

We therefore use spectral POD to decompose the sound field. In this case the kernel of the POD problem is the cross-spectral matrix $Spp(\theta_i, \theta_j, \omega)$:

$$Spp(\theta_i, \theta_j, \omega) =< p(\theta_i, \omega).p^*(\theta_j, \omega) >, \qquad (1)$$

where <> denotes ensemble averaging. The Fredholm integral is solved one frequency at a time, providing us with frequency-dependent eigenvalues and eigenvectors. The spatial phase of the soundfield is thus captured at each frequency, and this information is contained in the shapes of the eigenfunctions (which are complex). The temporal phase is lost, but it can be recovered later by projecting the original data onto the eigenfunctions.

The frequency dependent eigenvalues are shown in figure 3(a). We see that the first eigenmode captures a very large portion of the energy, particularly at the peak frequency, and has a "peaky" spectral shape similar to the LSS. In the same idea, Nance & Ahuja [13] used data from 2 or 3 phase correlated microphones to semi-independently extract the LSS and FSS spectral shapes. The higher order modes are more broadband. The directivity of the modes is shown in figure 3(b). Mode 1 clearly dominates the downstream radiation, and has a shape characteristic of a wave-packet type source. The remaining modes have gradually changing spectral shapes and directivity patterns. This decomposition certainly appears to isolate an important dominant source mechanism with spectrum and directivity of the form of the first POD mode ; however, there is no clear second mode which might correspond to something which could be clearly associated with a second, statistically independent 'source' mechanism.

3.2 Wavelet analysis

An analysis of the pressure signals by means of a continuous wavelet transform is performed so as to extract high-energy, intermittent events. The equations used to perform such a transformation are here briefly presented. For more information the reader can refer to Farge[14].

The continuous wavelet transform of the pressure signal is :

$$\tilde{p}(s,t) = \int_{-\infty}^{\infty} p(\tau)\psi(s, t-\tau)d\tau, \qquad (2)$$

where s is the scale of the wavelet function. A Paul wavelet is used in this study, defined for s = 1 with an order m as (see Torrence et al.[15] for more details) :

$$\psi(1, t-\tau) = \frac{2^m i^m m!}{\sqrt{\pi(2m)!}}[1 - i(t-\tau)]^{-(m+1)}. \qquad (3)$$

The motivation for using this complex wavelet is that it better preserves the integrity of something which can be associated with a single 'event', on account of that fact that the real and imaginary parts of the wavelet allow both high energy peaks and zero crossings associated with a given signature to contribute continually over an integral scale over which the event is active. Real wavelets will tend to break such single events into unphysical sub-events. The shape of Paul's wavelet for $m = 4$ in the temporal domain is shown in figure 4.

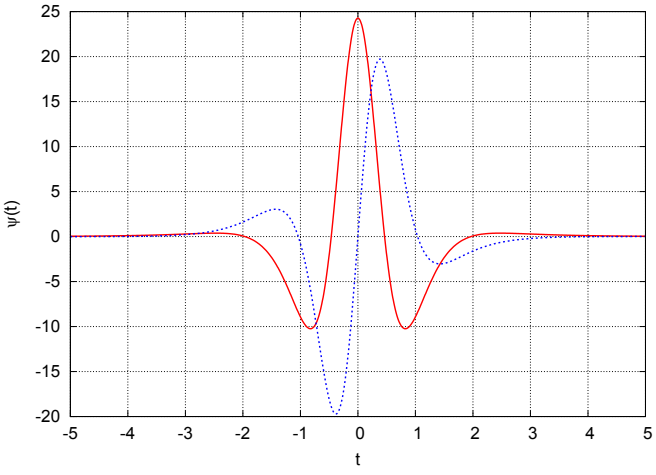

FIG. 4: Paul's wavelet ; —— real part ; – – – imaginary part.

An example of scalograms of the pressure signals measured at 30° and 90° is shown in figure 5. For clarity, we only present a short time interval (0.1 s) of the signal (the original signal has a temporal length of ten seconds, and filtering is performed over the entire duration of

the measurement). Before performing the wavelet transform, the signals are bandpass filtered to eliminate non-physical frequencies (lower than the cutoff frequency of the windtunnel for instance) and they are then normalised by the rms pressure at each angle so as to have a unit energy regardless of the observation angle. Also note that the scale s is converted to a pseudo-frequency f as in Torrence et al.[15] (which we then convert to a pseudo-Strouhal number) :

$$f = (2m+1)/4\pi s$$
$$St = fD/U_j$$

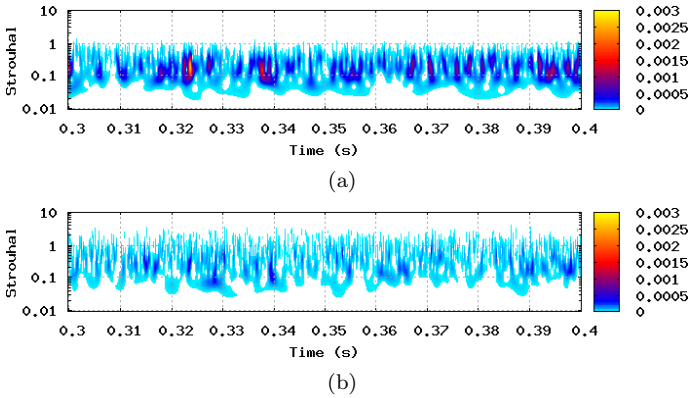

(a)

(b)

FIG. 5: Wavelet scalogram $|\tilde{p}(s,t)|^2$ at (a) 30° ;(b) 90°.

The 30° scalogram shows bursts of high-energy, temporally-localised activity, identified by the yellow/red spots. This is an indication of strong intermittent source activity where the downstream radiation is concerned. The 90° scalogram on the other hand does not have such marked intermittent activity (the colour scales are directly comparable on account of the normalisation which has been effected). As discussed earlier, there is a difference between downstream and sideline radiation, which is well captured by the similarity spectra LSS and FSS. We here see that, in addition to the different spectral shapes, there is also a marked difference in intermittency between radiation to high and low emission angles ; Fourier analysis necessarily misses this. If it amounts to an essential aspect of source mechanisms in jets, it needs to be explicitly modelled. Some work in this direction is reported by Sandham et al. [10] and Cavalieri et al [11].

We will now endeavour to quantify this intermittency as a function of polar angle. We do so by introducing a threshold parameter which we use to decompose the pressure signals into two components (we will use the ad-hoc terminology 'filtered-component' and 'residuum' to denote these)[1]. Filtering is performed using two criteria, each of which provides a different information regarding the temporal structure of the pressure signature considered : (1) Global Intermittency Measure ; and, (2) Local Intermittency Measure

Global Intermittency Measure

[1]this procedure is similar to that used by Samimy [8] to sort flow information into loud and quiet ensembles

The Global Intermittency Measure (GIM) allows us to identify temporally-, or scale-localised events which make large contributions to the overall fluctuation energy. The following filtering operation is effected :

$$\tilde{p_f}(\theta,s,t) = \begin{cases} \tilde{p}(\theta,s,t) & \text{if } |\tilde{p}(\theta,s,t)|^2 > \alpha \\ 0 & \text{if } |\tilde{p}(\theta,s,t)|^2 < \alpha \end{cases} \quad (4)$$

The threshold α has units of energy density in the wavelet domain. As the total energy of each signal is normalised, the integration of the energy density in time and in scale is equal to unity. However, the distributions of the energy density in the scalogram may be completely different. Thus, for a given value of the threshold, more energy will be retained by the filtering for a peaky scalogram than for a flat one, and the relationship between the total filtered energy and the threshold is a quantitative measure of how peaky is the scalogram. Peaks in the scalogram may arise on account of two kinds of signal characteristics : if a signal has intermittent bursts, there will be an energy concentration in the time direction of the scalogram ; if, on the other hand, a signal has a pure frequency, such as a sine wave, there will be a concentration in the scale direction. If both conditions are verified, we have high concentrations in a limited region in both s and t. In this case, this is due to a high correlation of the original signal with a particular scale during a limited time interval. Physically, this corresponds to the presence in the temporal time series of a high-amplitude acoustic wave-packet, whose shape is well described by the wavelet function. The GIM metric will tend to highlight such events.

Local Intermittency Measure

The LIM [14] is defined as follows :

$$I(\theta,s,t) = \frac{|\tilde{p}(\theta,s,t)|^2}{<|\tilde{p}(\theta,s,t)|^2>_t}, \quad (5)$$

where the $<>_t$ operator indicates an average of the scalogram in the t direction. As this average is performed independently for each scale, the local intermittency measure indicates, for a given scale, and regardless of its absolute energy density, if there are energy concentrations in the temporal direction ; an energy concentration purely in scale, such as in a sine function, leads to an intermittence measure equal to one for all s and all t, which indicates that there are no intermittent bursts.

The filtering based on the local intermittency measure is again defined based on a threshold β :

$$\tilde{p_i}(\theta,s,t) = \begin{cases} \tilde{p}(\theta,s,t) & \text{if } I(\theta,s,t) > \beta \\ 0 & \text{if } I(\theta,s,t) < \beta \end{cases} \quad (6)$$

The relationship between the value of the β threshold and the total filtered energy is, as in the case of the filtering based on the energy density of eq. (4) a quantitative measure of the peaks in the distribution of the local intermittency factor. This corresponds now to the presence in the temporal time series of acoustic wave-packets of high amplitude *in relation to the average energy for each scale* ; however, this amplitude may be low in relation to the global energy.

3.2.1 Results of wavelet filtering

An example of a result of the filtering operation is shown in figure 6 for a microphone at 30°. The value of alpha in this figure is such that the filtered signal retains 30% of the total fluctuation energy. Figure 7(a) shows the filtered scalogram at 30°. Figure 7(b) shows the 90° scalogram for a value of alpha which leads to retention of the same energy.

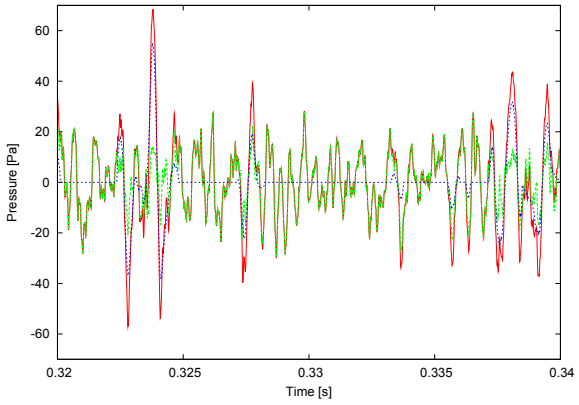

FIG. 6: Temporal pressure signals at 30° : —— baseline ; – – – "filtered" ; – – – "residuum".

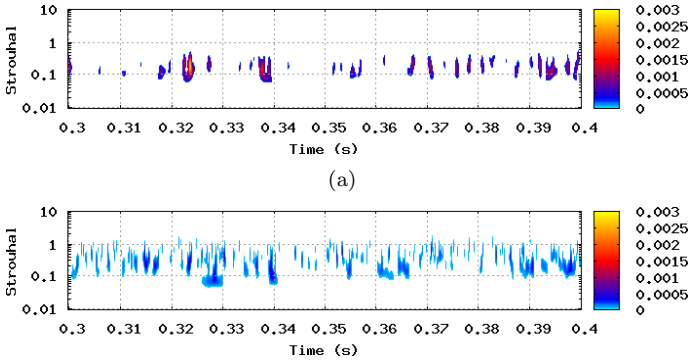

(a)

(b)

FIG. 7: Filtered wavelet $|\tilde{p}(s,t)|^2$ scalogram at (a) 30° ; (b) 90°.

The difference between the two filtered scalograms shows how the 30° signal receives contributions to its total fluctuation energy over shorter periods of high-amplitude activity ; the 90° signal showing a more homogeneous time-scale distribution.

Intermittency and fluctuation energy

Total energy is conserved under the wavelet transform and there exists the following equivalent of Parseval's theorem [15] for a given pressure signal localized at the angle θ :

$$\int_{\mathbb{R}} |p(t)|^2 dt = C_\psi^{-1} \int_{\mathbb{R}^+} \int_{\mathbb{R}} |\tilde{p}(s,t)| . |\tilde{p}^*(s,t)| \frac{dsdt}{s^2} \quad (7)$$

where $p(t)$ is the time pressure signal for a given polar position θ, $\tilde{p}(s,t)$ its continuous wavelet transform and C_ψ is a constant associated with the wavelet function which we use. As the pressure signals are normalised by the rms value, the integrated energy of the scalograms, regardless of the angle considered, is equal to one. Calculation of the energy after either GIM or LIM filtering, using equation 7, gives us the ratio of energy which is conserved. Figure 8 shows the relationship between filtered energy and α and β for each of the microphones. The GIM shows how the signals recorded in the angular

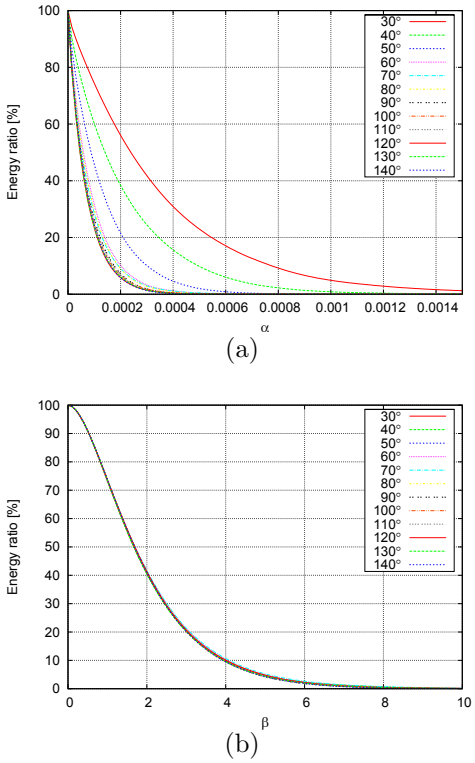

(a)

(b)

FIG. 8: Energy ratio (filtered/residuum) as function of polar angle ; (a) after GIM filtering ; (b) after LIM filtering.

range $60° \leq \theta \leq 140°$ comprise one family of curves. It is possible to conclude that these signals are characterised by similarly low levels of energetic intermittent events. In the angular range $30° \leq \theta \leq 50°$ on the other hand we see a gradual evolution from high levels of energetic intermittency at 30° to lower levels similar to those of the family of LEI (Low Energy Intermittency signals).

If we now consider the LIM-filtered data we see a very different picture : all of the curves collapse into a single family. This demonstrates that when we disregard contributions to the overall fluctuation energy, all of the scales of the farfield pressure signals are characterised by the same degree of temporal intermittency. This suggests that it is the acoustic efficiency of sources which is highly directional, rather than their absolute temporal structure.

Intermittency and active-time

We now study the impact of the filtering criteria on what we refer to as active time ; by active time we mean the percentage of the time-history for which non-zero

fluctuations are observed after the filtering operation has been applied. Figures 9 (a) and (b) show the result for the GIM and LIM filtering, respectively. The similarity with the previous result is striking : all microphones show a correlation between active-time and intermittent contribution to overall energy.

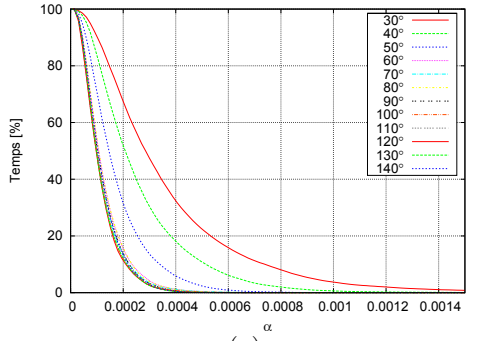

(a)

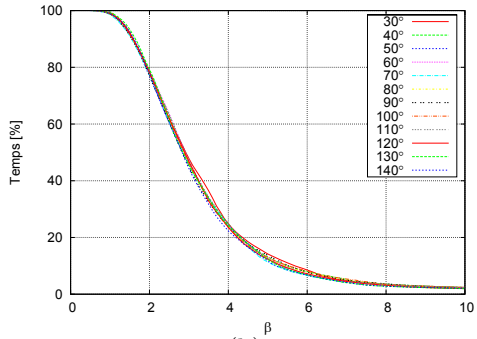

(b)

FIG. 9: Active time after : (a) GIM filtering ; (b) LIM filtering.

4 Conclusion

POD and wavelet filtering of data from the sound field of a Mach 0.9 round jet show that it is possible to identify two behavioural families : in the angular sector $30^\circ \leq \theta \leq 50^\circ$ the first POD mode captures virtually all of the fluctuation energy ; the temporal structure, as quantified by a Global Intermittency Metric, while not identical over this angular range, has a behaviour which is distinct from that observed at higher angles. In the second angular sector $\theta > 50^\circ$, while the POD analysis does not so clearly group the pressure signals into a single family of curves, the Global Intermittency metric does : fluctuations at these higher angles have identical characteristics in terms of their intermittent contribution to the overall fluctuation energy.

Acknowledgments

The present work was initiated during the 3^{rd} IFFC held in Poitiers in 2008. It was supported by SNECMA and CNPq, National Council of Scientific and Technological Development - Brazil.

Références

[1] Tam C., Viswanathan K., Ahuja K., Panda J. (2008) *The sources of jet noise : experimental evidence.* J. Fluid Mech., Vol.615, pp.253-292.

[2] Jordan P., Gervais Y. (2008) *Subsonic jet aeroacoustics : associating experiment, modelling and simulation* Exp. Fluids, Vol.44, pp.1-21.

[3] Goldstein M., Leib E. (2005) *The role of instability waves in predicting jet noise.* J. Fluid Mech., Vol.284, pp.37-72

[4] Crow S.C., Champagne F.H. (1971) *Orderly structure in jet turbulence.* J. Fluid Mech., Vol.48, pp.547-591.

[5] Michalke A., Fuchs H.V. (1975) *On turbulence and noise of an axisymmetric shear-layer.* J. Fluid Mech., Vol.70, pp.179-205.

[6] Juvé D., Sunyach M., Comte-Bellot G. (1980) *Intermittency of the noise emission in subsonic cold jets.* J. Sound Vibration, Vol.71, pp.319-332.

[7] Guj G., Carley R., Camussi C. (2003) *Acoustic identification of coherent structures in a turbulent jet.* J. Sound Vibration, Vol.259, pp.1037-1065.

[8] Hileman J., Thurow B., Carabello E., Samimy M. (2005) *Large-scale structure evolution and sound emission in high-speed jets : real-time visualisation with simultaneous acoustic measurements.* J. Fluid Mech., Vol.544, pp.277-307.

[9] Cavalieri A., Jordan P., Gervais Y., Wei M., Freund J. (2010) *Intermittent sound generation in a free-shear flow.* AIAA paper 2010-3963, 16^{th} AIAA/CEAS Aeroacoustics Conf., Stockholm, Sweden.

[10] Sandham N., Morfey C., Hu Z. (2006) *Sound radiation from exponentially growing and decaying waves.* J. Sound Vib., Vol.294, pp.355-361

[11] Cavalieri A., Jordan P., Agarwal A., Gervais Y. (2010) *A temporally-localized wave-packet model for subsonic jet noise.* AIAA paper 2010-3957, 16^{th} AIAA/CEAS Aeroacoustics Conf., Stockholm, Sweden.

[12] Jordan P., Gervais Y. (2005) *Modelling self- and shear-noise mechanisms in inhomogeneous, anisotropic turbulence.* J. Sound Vib., Vol.279, pp.529-555.

[13] Nance D., Ahuja K. (2009) *Experimentally Separating Jet Noise Contribution of Large-Scale Turbulence from that of Small-Scale Turbulence.* AIAA paper 2009-3213, 15^{th} AIAA/CEAS Aeroacoustics Conf., Miami, Florida.

[14] Farge M. (1992) *Wavelet transforms and their applications to turbulence.* Annual Rev. Fluid Mech., Vol.24, pp.395-458.

[15] Torrence C., Compo G. (1998) *A practical Guide to Wavelet Analysis.* Bulletin of the American Meteorological Soc., Vol.79, No.1.